A Cryogenic Current Comparator for the Absolute Measurement of nA Beams

Andreas Peters*, Wolfgang Vodel†, Helmar Koch†, Ralf Neubert†, Hannes Reeg*, Claus Hermann Schroeder*

*Gesellschaft für Schwerionenforschung, Darmstadt, Germany
†Institut für Festkörperphysik, Friedrich Schiller Universität, Jena, Germany

Abstract. A new type of beam transformer, based on the principle of a Cryogenic Current Comparator (CCC), was built to measure extracted ion beams from the SIS, the heavy ion synchroton at GSI. A current resolution of $0.006 - 0.065\ nA/\sqrt{Hz}$, depending on the frequency range, could be achieved allowing us to measure ion beams with intensities greater than 10^9 particles per second with high accuracy.

Numerous investigations were carried out to study the zero drift of the system which shows a strong exponential slope with two time constants. In addition, the influence of external magnetic fields was measured. Furthermore the microphonic sensistivity of the system was studied by measuring noise spectra of the detector's vibration and the output signal.

Measurements with neon and argon beams will be presented and compared with signals emitted from Secondary Emission Monitors (SEM). Another measuring function of the CCC-detector aims at the analysis of the beam's time structure to get information about beam spill fluctuations. With an extended bandwidth (0–20 kHz) of the detector system it is now possible to compare simulations of extracted beams from synchrotons with measurements of the CCC.

MOTIVATION

The main research topics of GSI are mid-range nuclear physics of heavy ions, atomic physics of highly-charged ions, biophysics (especially tumor treatment with carbon ions), and radioactive beams. Three different sources produce the ion beams for the UNILAC, the UNIversal Linear ACcelerator (Fig. 1). The highest energies at the UNILAC in the order of 10–20 MeV/u allow several experiments at the Coulomb barrier in the older experimental hall. One of these experiments aims at the production of new super-heavy elements, the last that was found is the element 112.

For higher energies up to 1–2 GeV/u a heavy ion synchroton (SIS) was added in 1989. High-energy beams can be kicked to the the experimental storage ring (ESR) for further atomic physics experiments using different cooling techniques.

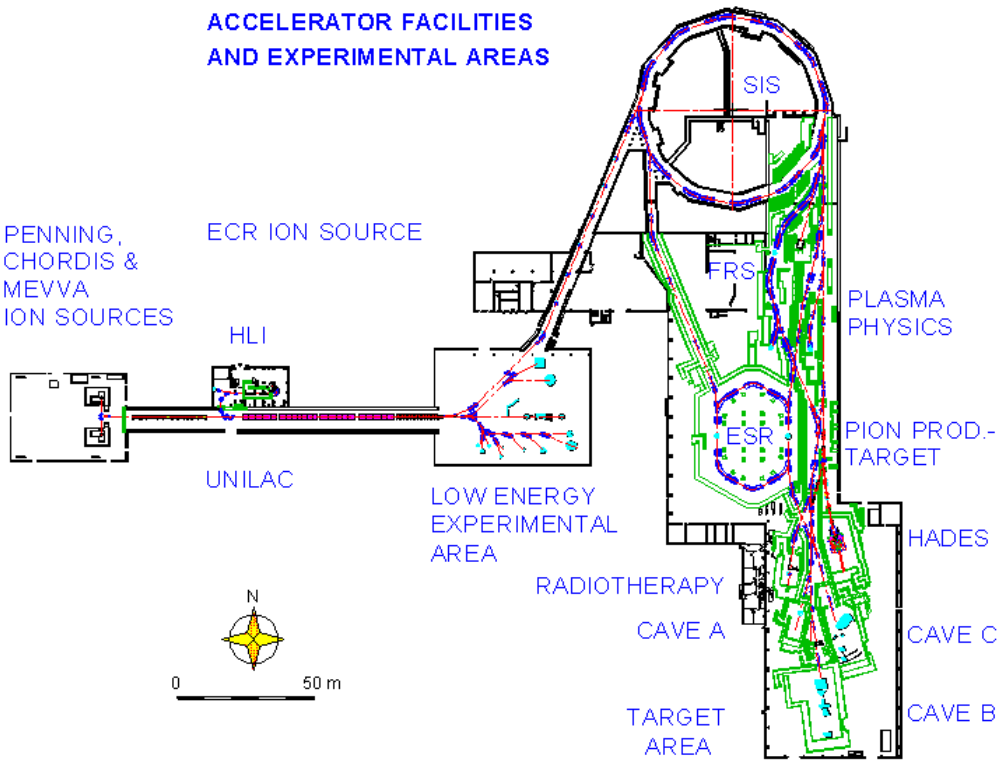

FIGURE 1. The GSI Accelerator Facilities.

On the other hand a lot of experiments use a resonant extracted beam for target radiation, e.g., to produce radioactive beams in the fragment separator (FRS). All these experiments will need higher beam intensities in future because of interest in measuring more exotic nuclei of smaller cross sections.

The GSI-accelerators UNILAC and SIS will be improved in the next three years so that the planned intensities of the SIS (defined by the incoherent space charge limit) can be reached [1]. To reach this aim a new injector consisting of RFQ- and IH-cavities will be installed instead of the old Wideroe-section. After the upgrade 2×10^{11} light ions (e.g., ^{12}C, ^{16}O, or ^{20}Ne) or 4×10^{10} heavy ions (e.g., ^{197}Au, ^{208}Pb, or ^{238}U) will be accelerated in the synchrotron corresponding to beam currents of about 300–500 mA at 1 MHz circulating frequency. Due to extraction times of 1–10 s the currents in the high-energy beam transport system could extend to some hundreds of nanoamps.

Besides new detectors for the UNILAC and the SIS, an expansion of the diagnostics for "high-intensity beams" in the beamlines to the new target hall was necessary. Possible detectors with relevant properties are as shown in Table 1.

Most detector principles are based on the interaction between the beam and material (e.g., scintillators, ionization chambers), so the beam is more or less distorted

TABLE 1. Detector Types and Properties

Detector principle	on-line	non-destruct.	radiation resistent	absolute calibration	suitable for vacuum
Nucl. trace counting	−	−	−	+	−
Faradaycup	+	−	+	+	+
Ionization chamber	+	−	+	−	−
Scintillation counter	+	−	−	+	−
Diamond detector	+	o	+	+	+
Sec. emission monitor	+	o	+	−	+
Residual gas monitor	+	+	+	−	o
Beam transformer	+	+	+	+	+

+ = yes/possible; o = possible only under favorable conditions; − = no/not possible

by scattering or energy loss. Diamond detectors represent a new and very interesting development in this field [2]. But all required properties are fulfilled only by beam transformers. Because the function of a DC transformer is based on both the modulation of a magnetic material and the observation of a shift of the hysteresis curve in the presence of a beam current through the pick-up coil, the limiting factor is the Barkhausen noise produced by wall-jumps of magnetic regions. To avoid this phenomenon no modulation of the core material is allowed.

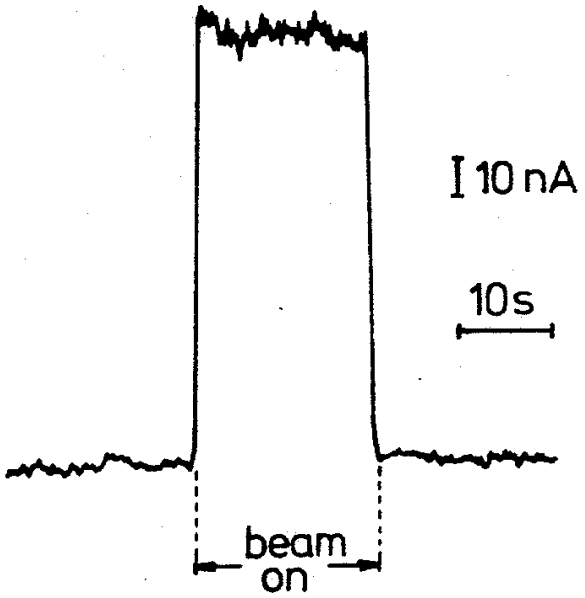

FIGURE 2. An electron beam current measured by a CCC at the PTB Berlin in 1977.

To reduce other noise effects, a cooling of the detector is often useful. Using low temperatures, modern superconductive detector principles could be taken into account as done in the early 70s by research groups in national standards laboratories. The first Cryogenic Current Comparator (CCC) was developed by I. K. Harvey in Australia 1972 [3]. A few months later a similar CCC was built at the Physikalisch-

Technische Bundesanstalt (PTB) in Berlin [4]. This group was the first which used a CCC based on SQUIDs for measuring beam currents. An 108 nA electron beam was generated by a Van de Graaff accelerator at 2.5 MeV (see Fig. 2 for their best measurement). For the beam current of about 100 nA the corresponding magnetic field is only 0.2 pT at a distance of 10 cm.

Because the accelerator at the PTB was shut down and the problems with the self-made SQUIDs were large the development of this device was stopped. But the first measurements showed that a CCC with SQUIDs works in an accelerator environment with rf background and large magnetic stray fields. Further developments with modern techniques seemed to be promising.

THE FUNDAMENTAL PRINCIPLES OF A CRYOGENIC CURRENT COMPARATOR

Figure 3 shows the construction principle of a CCC [5]. Two currents counterflow through a superconducting tube and introduce a differential current on the surface of this tube which can be measured outside the tube via the magnetic field by a SQUID, a highly sensitive magnetic sensor (see below).

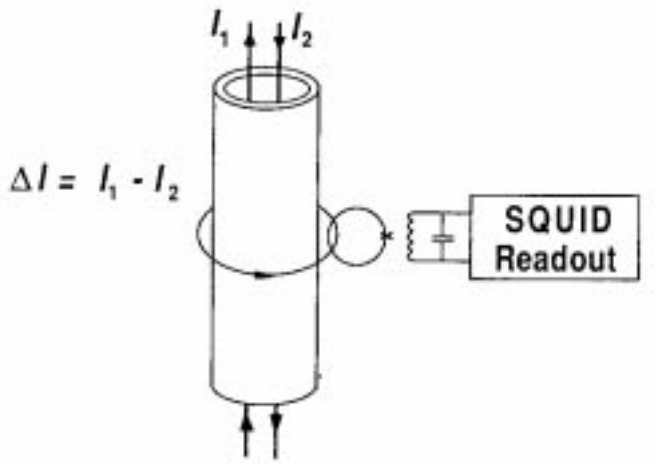

FIGURE 3. Construction principle of a cryogenic current comparator.

The ideal coupling is only obtained for an infinitely long shield cylinder but in practice this arrangement has to be replaced by inverting the shield cylinder into a toroidal geometry (see Fig. 4). To avoid a short circuit a little slit in the shielding is necessary. It is easy to recognize that only the azimuthal field of a current passing through the hole of this toroid can induce a magnetic field inside. Because of the geometry, all other field components are strongly weakened!

The mathematical treatment of the attenuation of different shield arrangements [6] gives the solutions shown in Table 2 (for geometries, see Fig. 5):

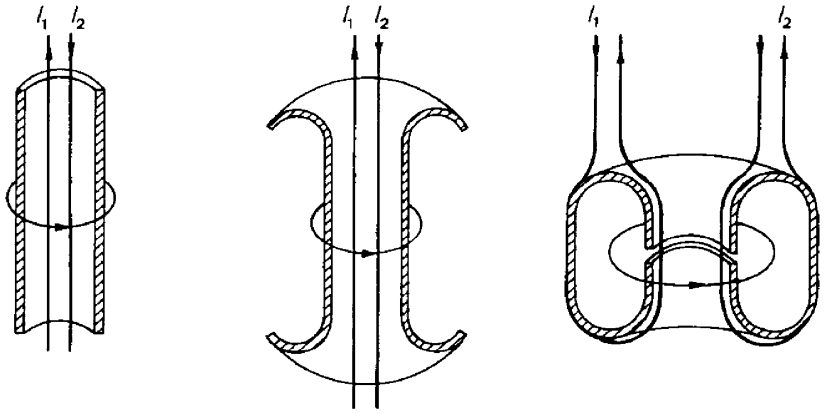

FIGURE 4. Transition of a cylinder geometry to a toroid geometry for a CCC.

TABLE 2. Shield Types and Their Attenuation Properties

Type	**Attenuation**
Coaxial cylinder	$A_{CC} = exp\{-\frac{2}{1+r_i/r_o} \cdot \frac{l}{r_a}\}$ $(r_a/r_i \leq 1,5)$
Simple cylinder	$A_{SC} = exp\{-1,84 \cdot \frac{l}{r_c}\}$
Ring cavity, type I	$A_{RC1} = \{\frac{r_i}{r_o}\}^2$
Ring cavity, type II	$A_{RC2} = 1$

r_i, r_o are inner and outer radii for coaxial cylinders and ring cavities of type I; r_c is the radius of the cylinder for simple cylinders; l is the length of the gap.

CCCs made of long (coaxial) cylinders have the advantage of high attenuation factors but they have only a small inner radius. A CCC consisting of ring cavities allows a larger inner radius which is necessary for proper functioning. The disadvantage of a smaller attenuation in this geometry can be compensated by using more cavities.

In addition to the magnetic shielding, a highly sensitive magnetic sensor is necessary to measure fields in the fT and pT ranges. Superconducting QUantum Interference Devices are sensors consisting of a superconducting ring with two weak links for the DC type. Two superconducting effects should be mentioned to under-

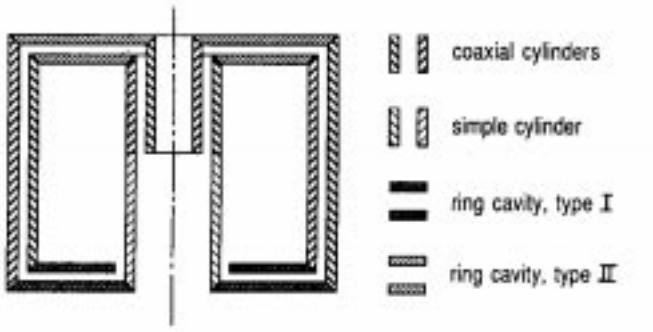

FIGURE 5. Classification of superconducting shielding geometries.

stand the function of a DC-SQUID:

- In a superconducting ring a quantization of the magnetic flux is observed:
  $\Phi_{mag} = n \cdot \Phi_0, \qquad n = 0, 1, 2, \ldots \qquad$ with $\Phi_0 = \frac{h}{2e} = 2.07 \times 10^{-15} Vs$
- In the presence of a weak link the so-called "DC Josephson Effect" appears (Figure 6):

  The affiliated wave functions of the Cooper pairs are:

$$\Psi_1(r) = |\Psi_1(r)|e^{i\varphi_1(r)}$$
$$\Psi_2(r) = |\Psi_2(r)|e^{i\varphi_2(r)}$$

  The two wave functions are coupled to each other due to the possibility of tunneling through the barrier. The solution of this coupled equations is:

$$I(t) = I_0 \cdot sin(\tfrac{2eV_0}{\hbar}t + \varphi_0)$$

  For zero voltage across the junction there is a DC current $I = I_0 \cdot sin\varphi_0$ which can assume any value between $-I_0$ and $+I_0$.

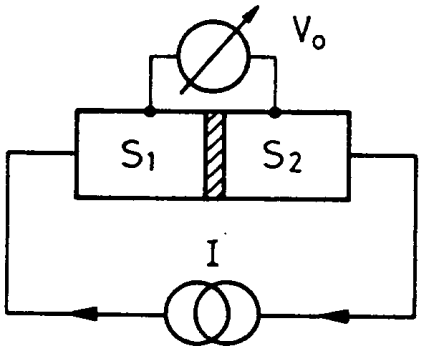

FIGURE 6. Schematic arrangement of a Josephson junction.

A superconducting loop consisting of two Josephson junctions in parallel exhibits interference phenomena. In the DC case the total current is

$$I = I_a + I_b = I_0(sin\varphi_a + sin\varphi_b).$$

When a magnetic flux Φ_{mag} threads the area of the loop, the phases differ by

$$\varphi_a - \varphi_b = \tfrac{2e}{\hbar} \oint \vec{A} \cdot \vec{ds} = \tfrac{2e}{\hbar}\Phi_{mag}.$$

With $\varphi_0 = (\varphi_a + \varphi_b)/2$ the current I is

$$I = I_0 \cdot sin\varphi_0 \cdot cos(\tfrac{e}{\hbar}\Phi_{mag}).$$

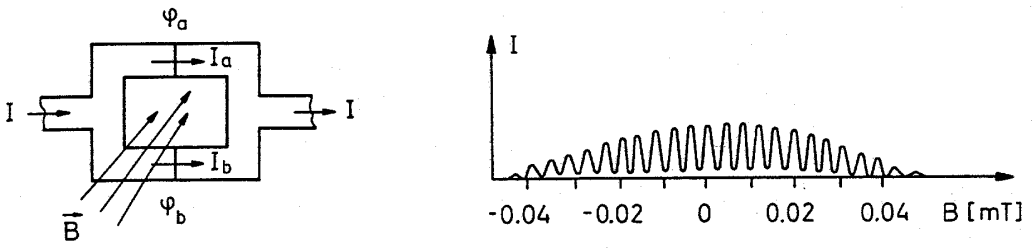

FIGURE 7. SQUID current dependence on an external magnetic field.

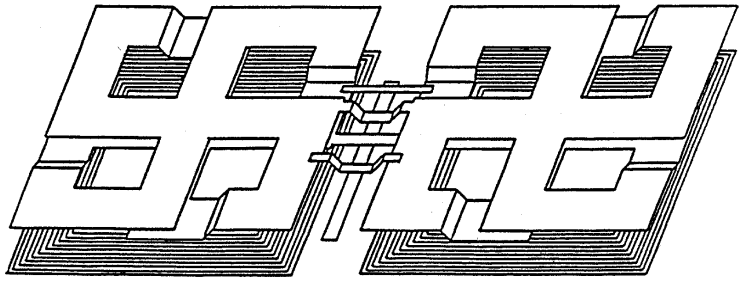

FIGURE 8. Modern SQUID layout (schematically).

Figure 7 shows the result of this function which is the same as the interference pattern of a double slit in optics. The output voltage of the SQUID is directly coupled to the magnetic flux Φ_{mag} caused, for example, by a beam passing a pickup coil of a CCC.

Today DC SQUIDs are fabricated like micro chips with multilayer techniques. Figure 8 shows a simplified drawing of the layout of the DC SQUID UJ 111 designed and manifactured by the Institute of Solid State Physics at the Friedrich Schiller University, Jena, Germany. To suppress the influence of external magnetic fields a gradiometric design was chosen [7].

To read out the signals generated by a SQUID chip, special electronics are required [8]. This consists of a low-noise preamplifier, a bias current source, a lock-in detector (with a modulation frequency of 125 kHz) followed by an integrator and filter module. The scheme of the DC SQUID electronics is shown in Figure 9.

THE DESIGN OF THE GSI PROTOTYPE-CCC

At the project's start in 1992, the following requirements for the detector were defined:

- Cryostat:
  - Working temperature: 4.2 K (liquid helium temperature)
  - Boil-off rate: $\leq$ 5 l liquid helium per day
  - A "warm hole" for the passing ion beam with 100 mm aperture

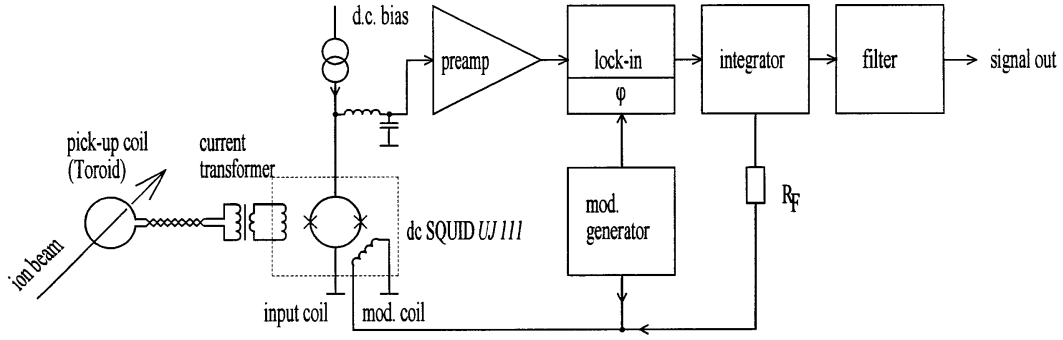

FIGURE 9. Scheme of the DC SQUID electronics.

- Magnetic shielding highly efficient against stray fields
- Resolution of the whole system: $\leq 1\ nA/\sqrt{Hz}$
- Current zero drift: $\leq$ 1nA/min
- Maximum bandwidth of the output signal: 0–5 kHz
- Maximum range: 10 μA
- Accuracy of the whole measurement system: $\pm$ 5 %

To meet these requirements a special liquid helium bathcryostat with a "warm hole" of Ø 100 mm for the passing ion beam was designed. The outer radiation shield consists of a superinsulated copper vessel cooled to about 40 K by a Gifford-McMahon refrigerator. Figure 10 shows the mechanical setup of the cryostat which is nearly 1.2 m high and has a diameter of about 0.66 m.

In Figure 11 the design of the magnetic shielding and the input coil is shown. The input coil — a single winding formed as a toroid with a VITROVAC core — is made from niobium while the meander shape shielding is produced from lead plates and tubes insulated by teflon foil. An attenuation factor of 2×10^{-9} for external background fields (non-azimuthal) was calculated. The whole detector is mounted on a carrier tube with a ceramic gap to prevent parasitic wall currents.

The DC SQUID head designed and manifactured by the Friedrich Schiller University, Jena, Germany (see Fig. 12) is directly attached to the magnetic shielding whereas the other parts of the system — the preamplifier and the SQUID controller — are mounted outside the helium dewar.

MEASURED PARAMETERS

Cryogenic Performance

Several steps are necessary to cool down the cryostat and to fill it with liquid helium. Because the LHe-container including the detector system weighs about

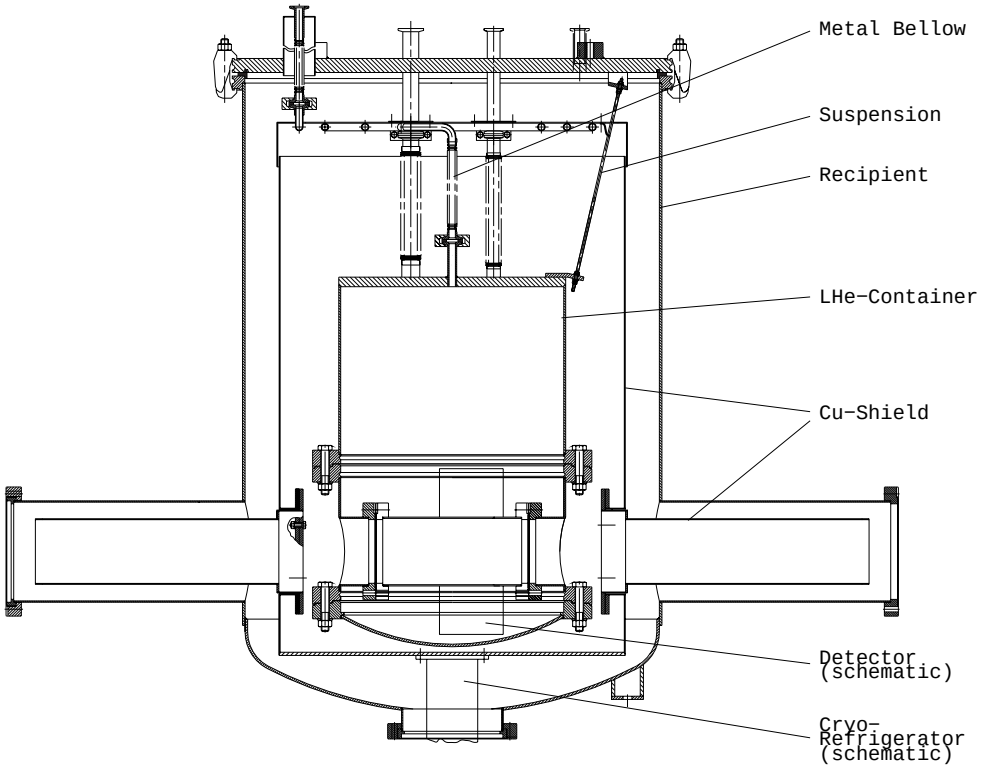

FIGURE 10. Design of the special bath-cryostat for the CCC.

100 kg this process takes about three days. As a result of continuous measurements of the helium level a minimum boil-off rate of 5.6 l LHe/d was observed. This corresponds to a heat loading of the LHe-vessel of 170 mW and is in good agreement with the theoretical calculated power consumption of about 125 mW.

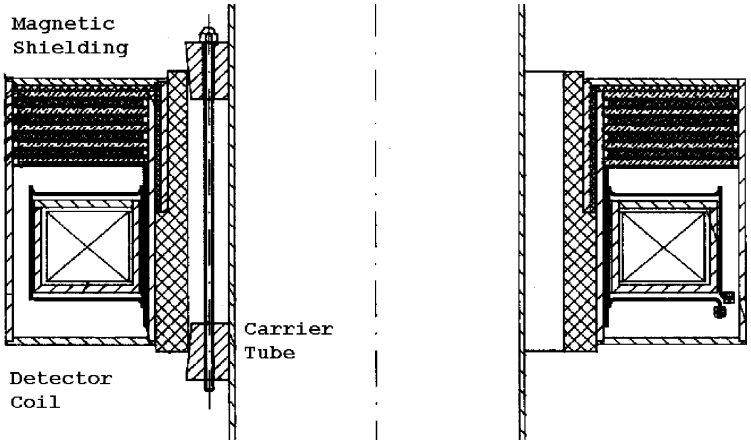

FIGURE 11. Design of the magnetic shielding and the input coil.

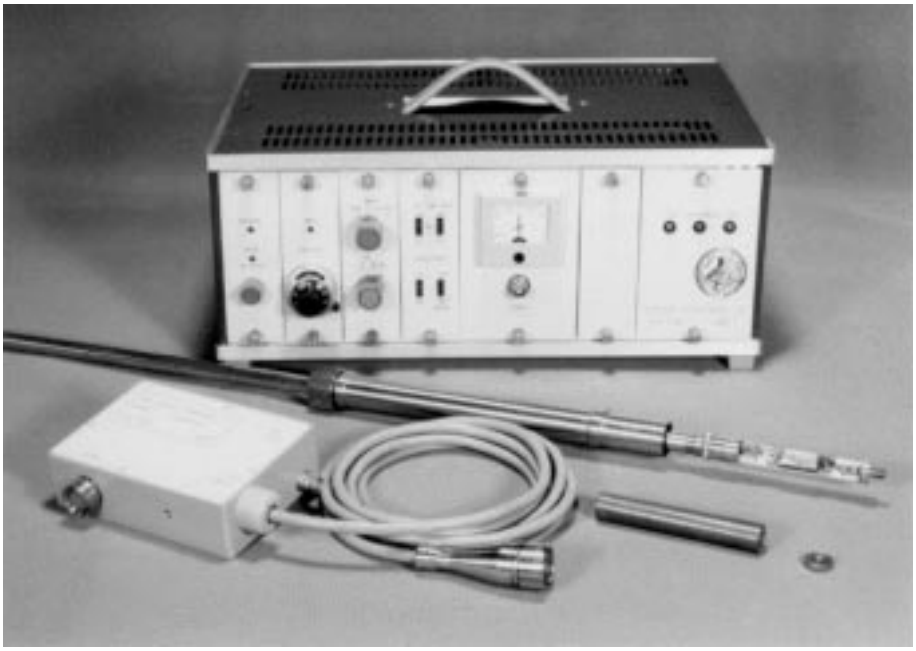

FIGURE 12. DC SQUID system model 4.

Current Sensitivity

A first output signal was observed by feeding a 10-nA test pulse of a calibrated current source (Keithley model 261) into the calibration winding through the pickup coil (see Fig. 13). For this measurement a bandwidth of 500 Hz was chosen.

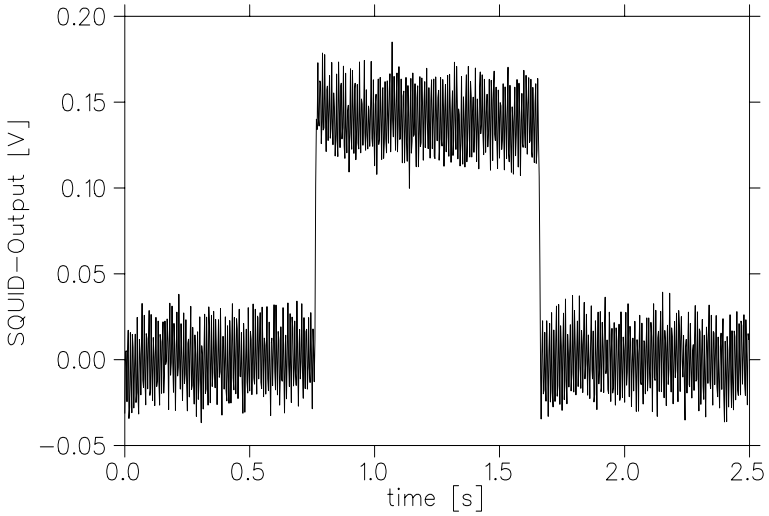

FIGURE 13. Measurement of a 10 nA test pulse.

In Figure 14 the plotted output voltage of the SQUID electronics as a function of the calibration current is presented. The current sensitivity of the detector system was determined to 181.0 nA/ϕ_0, the linearity error is smaller than 0.5 %

(1 ϕ_0 corresponds to an output signal of 2.5 V in the most sensitive range of the SQUID system). During the measurements the refrigerator was switched off to avoid microphonic effects and magnetic interference (see below).

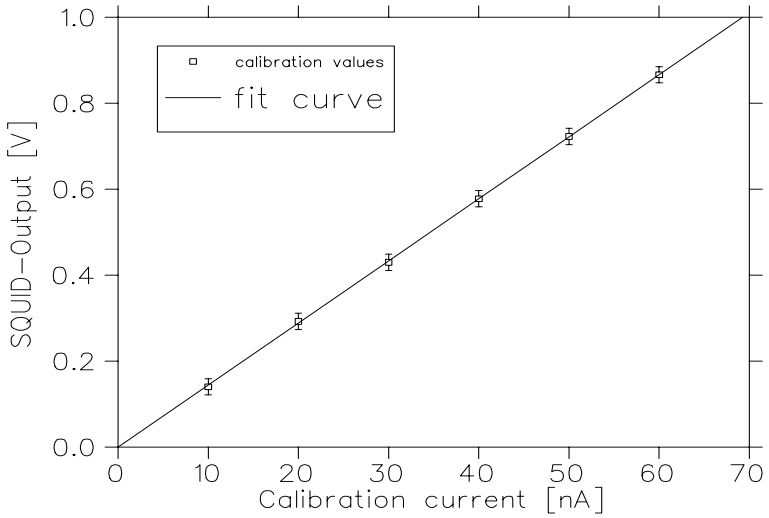

FIGURE 14. Calibration curve of the CCC.

Noise Level and Current Resolution

To determine the current resolution a noise spectrum (with open input) was taken. The noise level of 0.08-0.9 $\mathrm{mV}_{RMS}/\sqrt{Hz}$ corresponds to a current resolution of 0.006-0.065 $\mathrm{nA}/\sqrt{Hz}$, depending on the measurement frequency (see Fig. 15). The cut-off frequency of the system was found at about 10 kHz (small signal mode).

Current Zero Drift

At the beginning of each test the output signal of the CCC shows a strong zero drift. It was supposed that residual flux in the core of the coupling coil fades slowly away because of imperfect superconducting contacts in the input circuit. To study this effect the detector was cooled down to 4.2 K over a period of about 100 hours. The results of the long-term measurement are shown in Fig. 16. The curve is fitted by the sum of two exponential functions where the time constants are 3.3 hours and 30.8 hours. The shorter time constant is caused by a thermal effect. After a cooling time of about 100 hours the zero drift drops to values under 0.5 mV/s ($\cong$ 35 pA/s current drift), during another test run a minimum value of 0.23 mV/s ($\cong$ 16 pA/s current drift) was achieved.

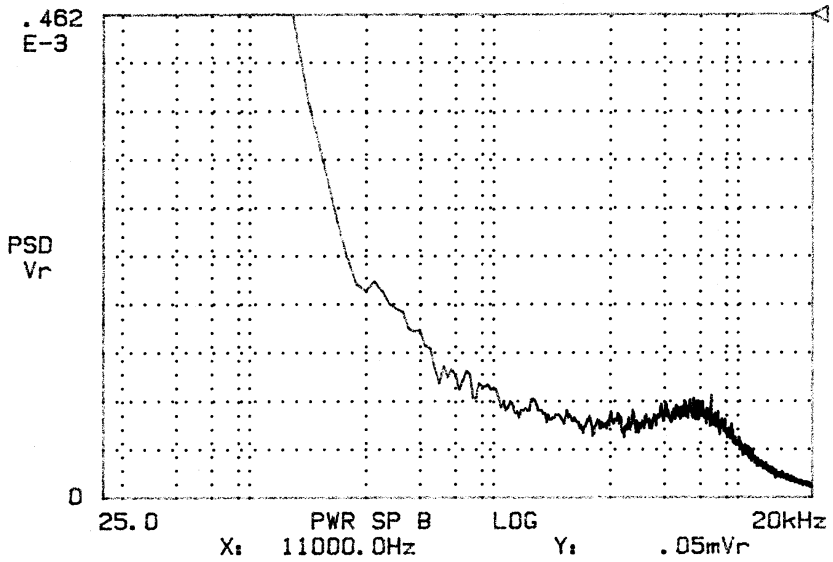

FIGURE 15. Noise spectrum of the CCC.

Influence of External Magnetic Fields

Further measurements were carried out to study the influence of external magnetic fields. A field of 10^{-5} T produced by Helmholtz coils yields the following apparent currents:

$\vec{B} \parallel \vec{I}$	3.3 nA
$\vec{B} \perp \vec{I}$	22 nA

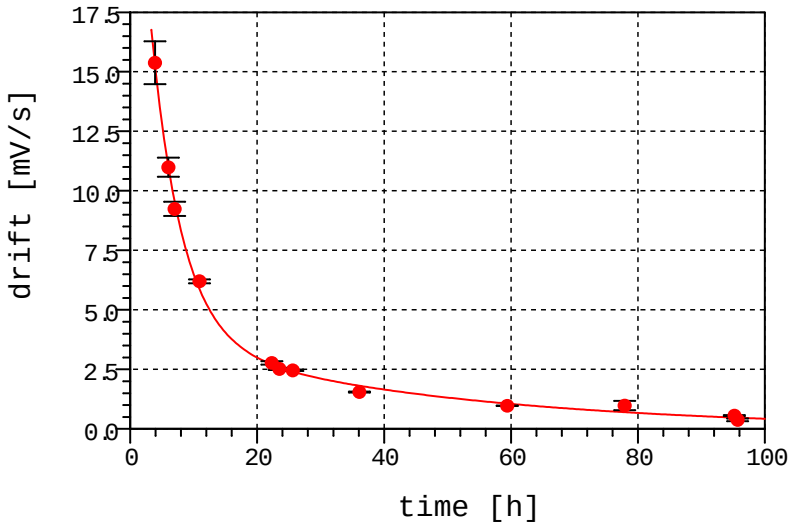

FIGURE 16. Long-term measurement of the current zero drift.

These values are 1–2 orders of magnitude higher than expected, but small enough to allow tests under real conditions in the beam line of the beam diagnostics test stand.

Influence of External Vibration

Numerous investigations with an accelerometer were carried out to study the microphonic sensistivity of the detector system. For this test the Gifford-McMahon

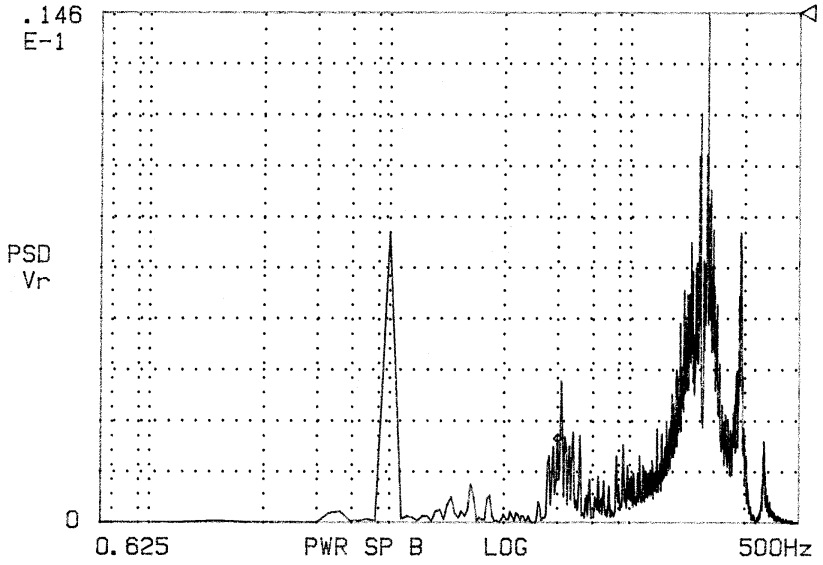

FIGURE 17. Spectrum caused by the influence of external vibrations.

refrigerator was switched off because of the strong mechanical influences. If the vacuum pumps close to the detector are switched on during measurements, an unavoidable mechanical influence in an accelerator environment besides vibrations of the building, the noise spectrum (see Fig. 17) shows several characteristic lines. Besides the disturbing electrical interferences caused by the mains (50, 100, and 150 Hz) there are some other peaks in the range around 70 Hz and corresponding harmonics at higher frequencies caused by mechanical resonances of the dewar.

Measurement results were taken into account for the design of the vibration-insulated installation of the detector in the test beam line. The device is mounted on three rubber bearings, and vibrations of the beam pipe are damped by metal bellows on each side of the CCC. Figure 18 shows the CCC at the beam diagnostics test bench.

MEASUREMENTS OF NEON BEAMS

First measurements were carried out in May 1996 with a $^{20}Ne^{10+}$ beam at 300 MeV/u. About 4×10^{10} particles per machine cycle were accelerated in the SIS

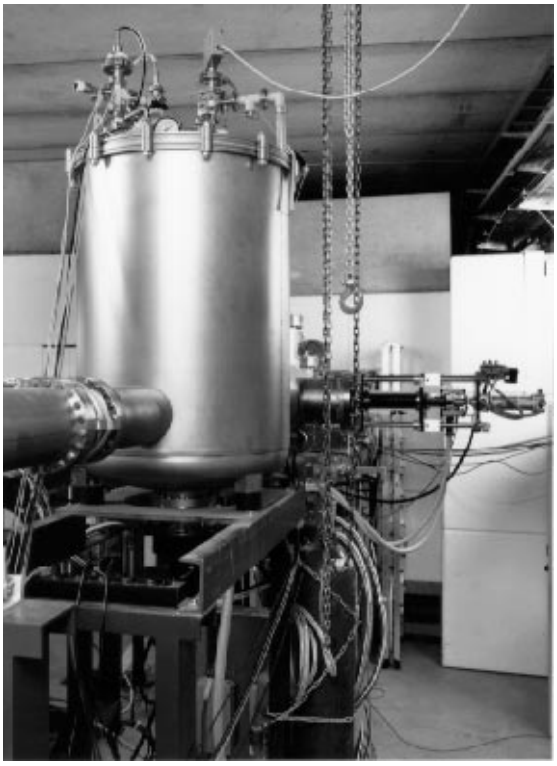

FIGURE 18. Cryostat with detector system at the beam diagnostics test bench (Photo: Achim Zschau, GSI).

and were extracted to the beam diagnostics test bench with a transmission of about 50%. A typical measurement is shown in Figure 19. The extracted ion beam shows a strong modulation with current peaks up to 35 nA while the average current is about 12 nA.

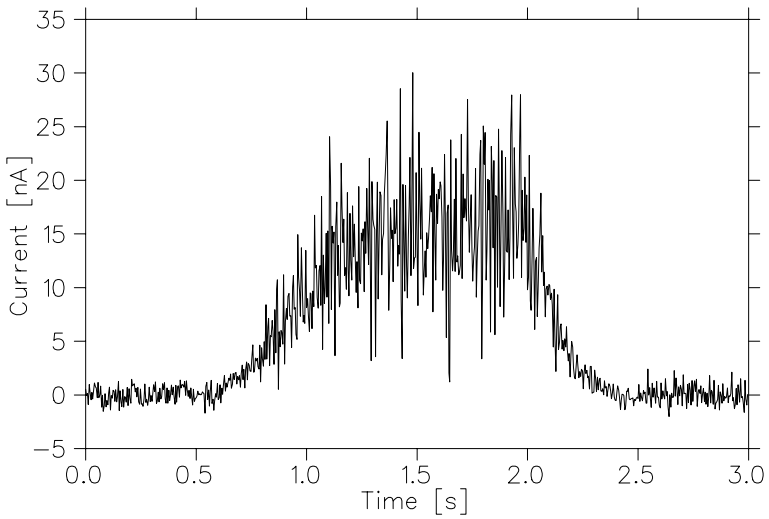

FIGURE 19. Measurement of a 300-MeV/u neon beam extracted of the SIS.

Calibration of SEMs versus CCC

A secondary electron monitor [9] made of three aluminum plates is mounted closely behind the CCC to provide a comparable measuring device. Again for a $^{20}Ne^{10+}$ beam at 300 MeV/u the spill rate was determined by a SEM and the CCC detector. Within a 5% error of each measurement system this plot shows a good linear correlation of the datas (see Fig. 20).

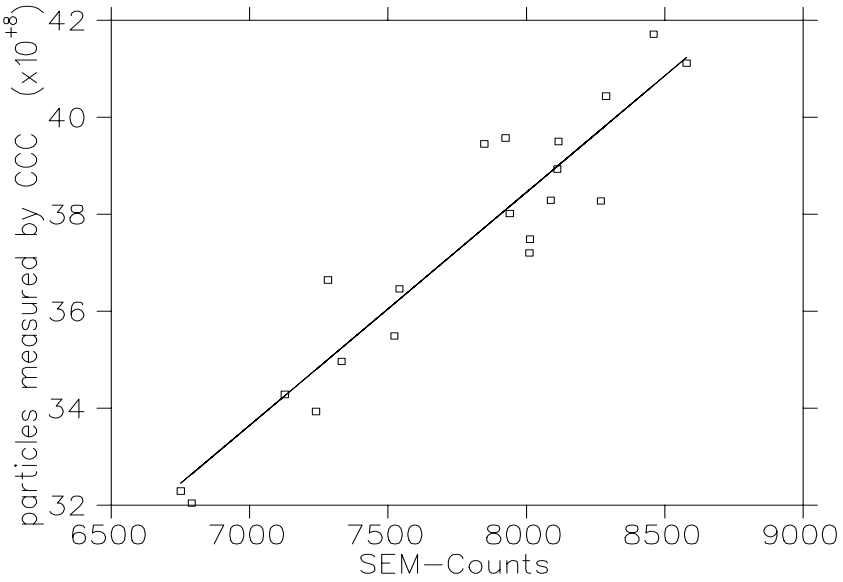

FIGURE 20. Calibration curve, CCC versus SEM data.

For the determination of the particle rate measured by the SEM the energy loss of the ions inside the Al material is calculated using the Ziegler formalism [10]. For the specific yield — the amount of detectable secondary charge per unit energy loss — a formula was used that shows a slight dependence on the nuclear charge of the incoming ions [11]. Further comparative measurements with various ion species are necessary to verify this behaviour.

FIRST ANALYSIS OF THE STRUCTURE OF EXTRACTED ION BEAMS

With a broadened bandwidth of 20 kHz more details of a Neon beam can be observed. Figure 21 shows the "burst" structure of the extracted ion beam.

M. Pullia studied this behaviour of the resonant extraction process [12]. Simulations assuming a monochromatic beam with a ripple on the power supplies showed a similar spill structure compared to the CCC measurement (see Fig. 22).

To find out the main accelerator components responsible for the ripples, a frequency analysis was calculated which is shown in Figure 23. The strongest peaks at

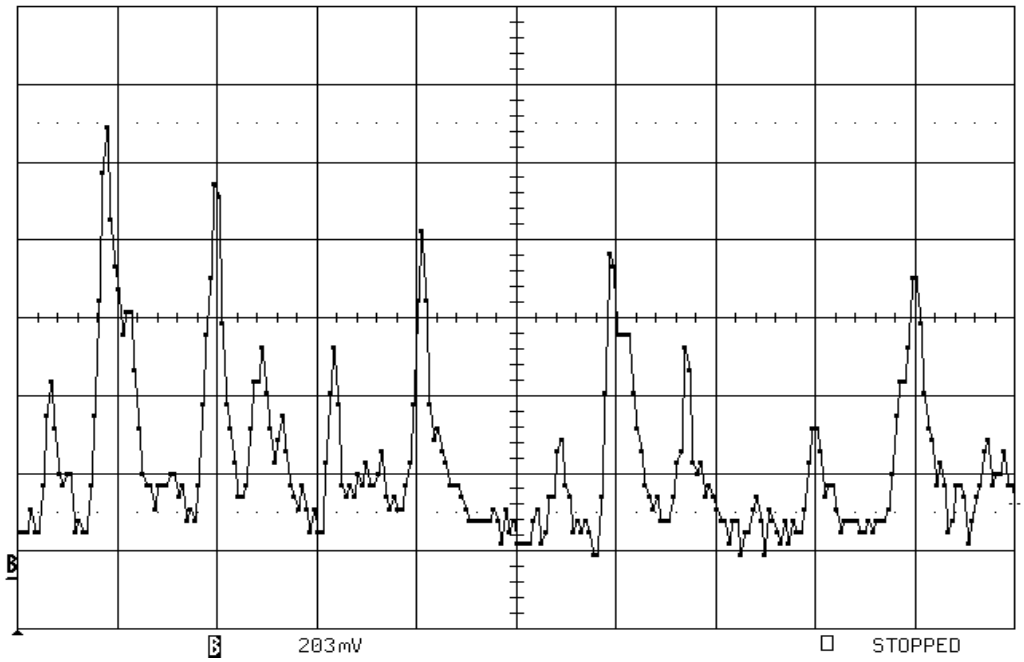

FIGURE 21. Detailed view of an extracted neon beam (x-axis: 0.5 ms/div.; y-axis: 0.21 V/div. = 15.2 nA ion current per div.).

1200Hz and 600 Hz (and the corresponding harmonics) are correlated to the characteristics of the 12-way rectifier bridges of the dipole and quadrupole power supplies

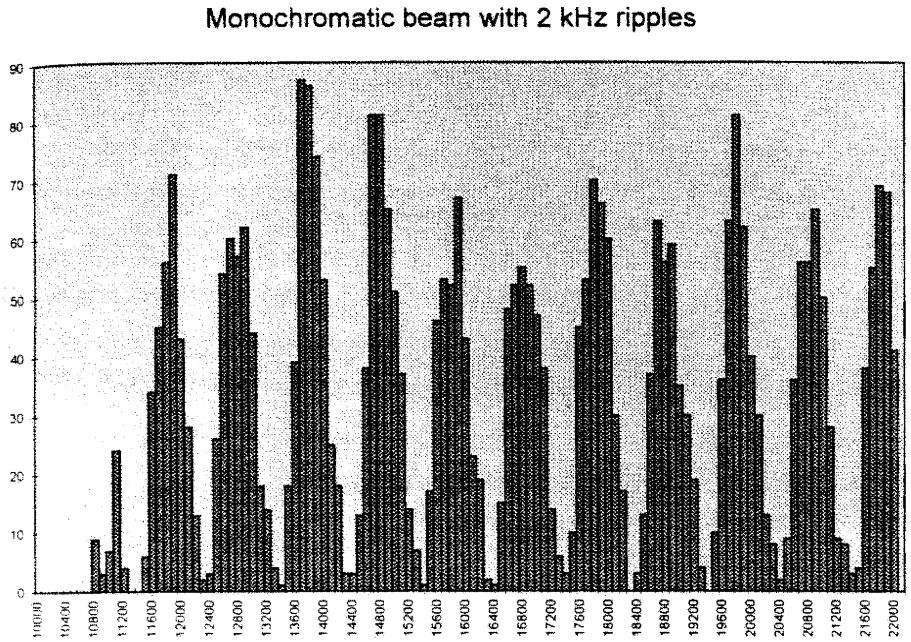

FIGURE 22. Simulation of a resonant extracted beam from a synchroton by M. Pullia.

in the SIS. The sextupole power supplies are possible further sources responsible for the ripples, especially in the lower frequency range. Additional investigations are necessary to minimize these effects.

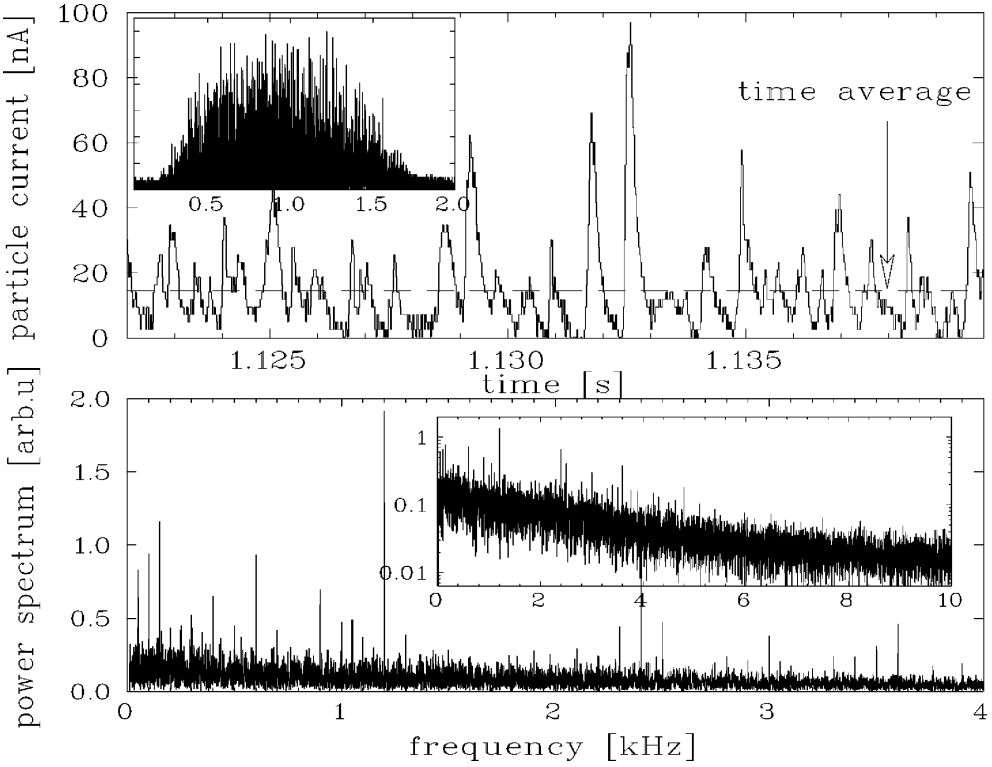

FIGURE 23. Frequency analysis of the resonant extracted beam.

FURTHER DEVELOPMENTS AND OUTLOOK

Further improvements will be done in the near future:

- A higher dynamic range of the DC SQUID electronics is needed. Until now the slew rate is limited to about 5000 ϕ_0/s ($\cong$ 1 nA/μs). If the current rise exceeds this value the feedback circuit of the CCC electronics becomes unstable and negative spikes can be observed. To avoid these instabilities a new version of the SQUID electronics is in preparation. The development aims at a higher slew rate combined with an increased bandwidth.
- In addition, an automatic offset correction will be installed to minimize the zero drift during a typical measurement interval of 1–10 s.
- Because of the strong vibrations of the Gifford-McMahon refrigerator, a prototype of a pulse tube cooler was used which produces a factor of 1000 less disturbance [13].
- For an autonomic detector, a small and cheap helium reliquifier is needed.

CONCLUSION

A new type of beam transformer using the measurement principle of a CCC and based on a high performance DC SQUID was developed and successfully tested in the extraction beamline of the SIS at GSI. Beam currents down to 1 nA can be measured nondestructively. Because of the high resolution of the CCC the beam structure can be analyzed within a bandwidth of 10 kHz.

In addition to the device's extremely high measurement sensitivity the most important advantage is greatly reduced effort for absolute calibration.

REFERENCES

1. Blasche, K., "Status Report on SIS-ESR," in *Proceedings of the Fourth European Particle Accelerator Conference (EPAC94)*, p. 133, London (1994).
2. Moritz, P., E. Berdermann, K. Blasche, H. Stelzer, and F. Zeytouni, "Diamond Detectors with Subnanosecond Time Resolution for Heavy Ion Spill Diagnostics," these proceedings.
3. Harvey, I. K., "A precise low temperature dc ratio transformer," *Rev. Sci. Instrumen.*, vol. 43, p. 1626 (1972).
4. Grohmann, K., D. Hechtfischer, J. Jakschik, and H. Lübbig, "A cryodevice for induction monitoring of dc electron or ion beams with nano-ampere resolution," in: *Superconducting quantum interference devices and their applications*, Walter de Gruyter & Co., p. 311 (1977).
5. Gutmann, P., and H. Bachmair, "Cryogenic Current Comparator Metrology," in *Superconducting Quantum Electronics*, V. Kose, Berlin, Heidelberg, New York: Springer-Verlag (1989).
6. Grohmann, K., D. Hechtfischer, J. Jakschik, H. Lübbig, "Field attenuation as the underlying principle of cryo current comparators," *Cryogenics* 16, pp. 423–429 (1976).
7. Vodel, W., and K. Mkiniemi, "An ultra low noise SQUID system for biomagnetic research," *Measurement Science and Technology*, Vol. 3, No. 2, pp. 1155–1160, December 1992.
8. Koch, H., W. Vodel, and T. Döhler, "DC-SQUID CONTROL 4 Instruction Manual," Jena, Germany (1990).
9. Forck, P., P. Heeg, and A. Peters, "Intensity measurement of high energy heavy ions at the GSI facility," in *Proceedings of the Seventh Beam Instrumentation Workshop*, workshop held at Argonne, May 1996; AIP Conference Proceedings 390.
10. Ziegler, F. J., *The Stopping Power and Ranges of Ions in Matter*, Vol. 5, Pergamon Press (1980).
11. Junghans, A. and K. Sümmerer, GSI, private communication.
12. Pullia, M., "Time Profile of the Extracted Spill," in *Proton-Ion Medical Machine Study*, CERN-Report, September 1996.
13. Häfner, H.-U., Leybold Vakuum GmbH, Cologne, Germany, private communication.